UC Davis
UC Davis Previously Published Works

Title
Broadband, freeform focusing micro-optics for a side-viewing imaging catheter.

Permalink

Journal

ISSN

Authors
Bec, Julien
Li, Cai
Marcu, Laura

Publication Date

DOI

Peer reviewed

Broadband, freeform focusing micro-optics for side-viewing imaging catheter

Julien Bec[1,2,3,4], **Cai Li**[1], **Laura Marcu**[1,*]

[1]Department of Biomedical Engineering, University of California, Davis, California 95616, USA

[2]Institute of Physical Chemistry and Abbe Center of Photonics (IPC), Friedrich-Schiller-University, D-07743 Jena, Germany

[3]Leibniz Institute of Photonic Technology, D-07745 Jena, Germany

[4] jbec@ucdavis.edu

Abstract

Successful implementation of a catheter-based imaging system relies on the integration of high-performance miniaturized distal end optics. Typically, compensation of chromatic dispersion, as well as astigmatism introduced by the device's sheath, can be addressed only by combining multiple optical elements, adversely impacting size and manufacturability. Here, we present a $300 \times 300 \times 800\ \mu m^3$ monolithic optic that provides high optical performances over an extended wavelength range (near UV-visible-IR) with minimal chromatic aberrations. The design of the optic, fully optimized using standard optical simulation tools, provides the ability to freely determine aperture and working distance. Manufacturing is cost effective and suited for prototyping and production alike. The experimental characterization of the optic demonstrates a good match with simulation results and performances well suited to both optical coherence tomography and fluorescence imaging, thus paving the way for high-performance multimodal endoscopy systems.

Fiber optic endoscopic probes have enabled breakthroughs in medical imaging because of their unique ability to reach deep into the human body. The combination of a low-profile side-viewing probe with a helical scanning pattern enables the rapid acquisition of images from luminal structures. Several techniques, such as optical coherence tomography (OCT) [1], spectroscopy [2], and fluorescence [3,4], have been successfully implemented following this principle, with applications for the detection of diseases in coronary arteries [1,5], gastrointestinal tract [1], as well as airways [6]. A key component for the successful implementation of fiber-based imaging techniques is the distal optical elements, used to direct and focus the optical beam, which should provide high optical performances in a small form factor. More specifically, the optic should provide the working distance and numerical aperture (NA) suitable for the application, with the introduction of minimal aberrations (spherical, chromatic). For typical optical systems, these design goals are addressed by combining multiple optical elements, but the scaling of such solutions to

*Corresponding author: lmarcu@ucdavis.edu.

sub-millimeter dimensions presents significant challenges. Additionally, certain elements specific to an endoscope, such as the transparent sheath typically used to separate the rotating imaging core from the surrounding environment, introduce astigmatism that should ideally be corrected [5]. In the last years, the combination of imaging modalities operating at different wavelengths has become more widespread [7-9], further highlighting the need for a distal end optic solution able to work over an extended wavelength range. The typical solutions for compact distal end optics, namely, gradient index (GRIN), and ball lens optics have been successfully implemented for the construction of low-profile side viewing endoscopes, but both present limitations.

Angle-polished fused ball lenses are fabricated by splicing a short section of no-core fiber with the main fiber, fused into a spheroid, and polished to provide an angled facet that deflects the beam via total internal reflection [10]. Different radii can be obtained in the axial and trans-axial directions to correct for astigmatism introduced by the device sheath. A suitable geometry of the spheroid is achieved empirically by optimizing the fusion process. Ball lens termination of large core multimode fibers (>100 μm) presents additional challenges, as the optical beam expansion is limited by the diameter of the no-core fiber This limitation has been reported when using the inner cladding of a double-clad fiber to deliver a fluorescence lifetime imaging (FLIm) excitation beam for a FLIm/OCT application [11]. Additionally, the use of the probe in liquids requires the addition of a cap, as both total internal reflection from the facet and focusing from the surface of the spheroid rely on a glass–air interface. This cap increases astigmatism, bulk, and complexity [12].

GRIN lenses are used in the visible and near-infrared ranges but common dopants such as silver ions present strong absorption and autofluorescence at 355 nm. Lithium is a UV-compatible dopant but limits in refractive index variations lead to a low NA of 0.2 [13]. This leads to long (>3 mm) elements not suitable for vascular use. Other limitations are strong chromatic aberrations, and an optical index profile that presents a circular symmetry thus does not enable the correction of astigmatism introduced by the device sheath [14,15]. The introduction of an additional cylindrical surface addresses this issue at the cost of increased complexity [14].

A 3D printed side-viewing optic for OCT application that relies on the reflection off a curved paraboloid surface was reported recently [16]. Although it shares many of the advantages of the solution proposed here, manufacturing is slow (>14 h per element). The design, based on total internal reflection, requires a cap that increases the overall bulk of the element. Additionally, the UV-curable photoresist material presents lower mechanical properties ($E = 4.5$ GPa), high absorption in the UV range, and overall lower optical performances than fused silica.

A different concept, using diffractive optical elements (DOEs) as alternatives to GRIN and ball lenses, has been addressing some of the issues of conventional optics for OCT [15]. DOEs are well suited to monochromatic, spatially coherent light, but the application of this technology to extended sources (such as multimode fibers) over a large wavelength range presents significant challenges [17].

Here, we present the design, fabrication, and characterization of a novel monolithic distal-end-optics concept able to address these issues: this design enables full control of the working distance, NA, correction of spherical aberration, as well as astigmatism introduced by the device's sheath and is inherently broadband, thus supporting the implementation of imaging modalities spanning the UV-IR range, such as OCT and FLIm in a single device.

The micro-optic described here consists of a fused-silica element terminated by a reflective curved back surface that performs beam focusing and reflection. In an ideal configuration, with light emitted from a point source (fiber core), the back surface could consist of an ellipsoid section where the first focus F1 is collocated with the source, such that all rays emitted from the source would converge to the second focus F2 [Fig. 1(a)]. In practical applications, the need to correct for sheath astigmatism and additional refraction of the light at the exit face (glass to water or air), led to the optimization of the back-surface geometry using optical simulation.

In this study, the geometry of the reflective surface was computed using Zemax (Radiant, Redmont, WA). The simulated model consisted of a fully filled 0.22 NA, 100 μm core multimode fiber, and a UV-fused-silica optical element of 300×300 μm^2 cross section, immersed in water and surrounded by a 0.96/1.25 mm inner/outer diameter TPX sheath (MX004, Mitsui Chemicals, Japan). The freeform reflective surface sag was defined as a conic asphere with an additional polynomial aspheric terms, where x and y are the transaxial and axial coordinates [Fig. 1(d)], and k, r, and a are the conic constant, normalization radius, and aspheric coefficient, respectively. [Eq. (1)]:

$$z = \frac{(x^2 + y^2)}{r\left(1 + \sqrt{1 - (1 + k)\frac{(x^2 + y^2)}{r^2}}\right)} + ax^2.$$

(1)

Numerical optimization of the surface parameters ($r = 1.323$ mm, $k = -48$, $a = .414$ mm^{-2}) and tilt (49.6 deg) was performed to provide 10 deg forward beam tilt and minimize the beam root mean square (RMS) radius at 1.5 mm distance [Fig. 1(b)].

The fabrication of the elements consisted of manufacturing a microlens-like array of the micro-optic back surface out of a fused-silica wafer using direct-write laser machining (PowerPhotonics, Fife, UK) [18]. After machining, a UV-enhanced aluminum coating was applied to provide broadband reflectivity in the UV-visible range (Laseroptik, Garbsen, Germany) [Fig. 1(c)]. Individual micro-optics were separated by a two-step dicing operation: the array was first cut into rows [Fig. 1(c) step 1], then individual elements [Fig. 1(c) step 2], and polished to length using diamond lapping sheets (LFXD, Thorlabs, Newton, New Jersey, USA) [Fig. 1(c) step 3].

The freeform optics were assembled with a 1 m length of 100 μm core multimode fiber optic (FVP100110125, Polymicro, Phoenix, Arizona, USA) using acrylate optical adhesive (OG603, Epotek, Billerica, Massachusetts, USA). This assembly was connected to the FLIm system reported earlier by our group [19] to perform the experimental characterization. The beam profile of the UV excitation beam was measured at different distances (0–4 mm) using

a 20× microscope objective and a 2,048 × 1,536 CMOS camera (MD310B-BS, AMScope), leading to a pixel size of 716 μm. Multimode beams do not necessarily present a Gaussian profile; therefore, the axial and transaxial beam profiles were fitted with different orders of super-Gaussian ($n = 2$ to 10) according to Eq. (2):

$$I(r) = I_0 \exp\left[-2\left(\frac{r}{w}\right)^n\right]. \tag{2}$$

For each distance, the super-Gaussian order that resulted in the least residual was used. The beam size was then computed as the full-width half-maximum (FWHM) of the fitted profile and compared with the beam profile computed from Zemax simulation performed in similar conditions (in air, no sheath) (Fig. 2).

The ability of the micro-optic design to improve fluorescence collection and lateral resolution was evaluated by coupling the probe with the system described in [4], and measuring fluorescence from a 200 μm polystyrene film for distances in a 0–4 mm range, as well as a 3 mm stent inserted in a fluorescent acrylic phantom. The results were compared to reference probes terminated with flat reflective prisms (Fig. 3).

The suitability of the micro-optic for intravascular OCT was evaluated by coupling the micro-optic *with* a 1 m length of double-clad fiber (DCF 9/105/125, Nufern, USA). After connection to a 1310 ± 55 nm swept source OCT engine from Axsun Technologies, we measured the beam profile for distances of 0 mm to 3 mm from the optic's top surface. The axial and transaxial beam profiles were fitted with Gaussian functions to extract the beam's FWHM (Fig. 4).

The optimization of the element's back surface geometry based on project-specific constraints (aperture, working distance, beam tilt, presence of a sheath) was straightforward. Manufacturing this geometry using direct laser machining did not present specific *challenges*, as the surfaces are smooth and present a low slope and a sag of less than 50 μm. No characterization of the machining accuracy was performed, but based on manufacturing guidelines provided by the manufacturer for low slope designs (<8 deg), a typical peak-to-valley form error of 0.5 μm is expected [20].

Due to the small dimensions of each optical element, a high number of elements (>900) could be included within the 15×15 mm^2 area available for machining. Application of the broadband reflective coating of the back surface on hundreds of optics at once was easy and cost effective. The following dicing and polishing operations were performed using a standard dicing saw and polishing equipment, readily available in a research environment.

Experimental characterization demonstrates that the micro-optics performances are in good agreement with the fluorescence excitation beam simulations performed to generate the design. Beam profiles at various distances, in the axial and transaxial directions, closely match simulated beam profiles and show negligible astigmatism with similar beam waist distance and beam divergence in the axial and transaxial directions.

These optics are well suited for FLIm, due to high UV transparency and low autofluorescence, and ability to work with large core multimode fibers. Here, we demonstrate that the micro-optic, combined with a 100 μm core fiber, presents a collection efficiency vastly superior to the same fiber terminated with a flat prism. It almost matches the collection efficiency obtained by an earlier version of the FLIm catheter combining a flat prism with a 200 μm core fiber that presents a four-fold larger cross section [4], while simultaneously enabling improvements in lateral resolution.

The same design demonstrates high performances for a 1310 nm OCT application: the waist position in the axial and transaxial directions is within 200 μm, and the beam presents similar divergence in both directions. Additionally, the beam FWHM is less than 20 μm in the focal plane.

The design presented here delivers superior optical performances over an extended wavelength range: optical rays travel in a straight line within the beam expansion region, and focusing is achieved via specular reflection off the back surface. The introduction of chromatic dispersion is limited to the refraction off the exit surface of the element. It is minimal, as the surface is flat and the beam presents a low divergence and angle of incidence. Therefore, this design compares favorably to refractive optics that are subject to significant chromatic aberrations, potentially corrected by the addition of multiple optical elements to compensate for wavelength dispersion. Finally, this design is suitable for use in air as well as water and is impervious to contaminations of the reflective surface. This proves valuable for integration into devices (Fig. 5).

In summary, compact, monolithic micro-optic elements that present an achromatic behavior over a large wavelength range, astigmatism correction, and straightforward optimization of aperture and working distances are easily manufactured. This combination of features could be obtained previously only by using a combination of optical elements. The direct-write laser machining of the freeform back surface does not require the upfront investment necessary for alternative techniques such as grayscale lithography or molding and can be easily outsourced. Several hundred optics can be manufactured from the same wafer and can include a large variety of alternative designs, making it suitable for R&D and production alike, thus enabling improvements in intraluminal imaging devices in both research and clinical environments.

REFERENCES

1. Yun SH, Tearney GJ, Vakoc BJ, Shishkov M, Oh WY, Desjardins AE, Suter MJ, Chan RC, Evans JA, Jang I-K, Nishioka NS, de Boer JF, and Bouma BE, Nat. Med 12, 1429 (2006). [PubMed: 17115049]

2. Gardner CM, Tan H, Hull EL, Lisauskas JB, Sum ST, Meese TM, Jiang C, Madden SP, Caplan JD, Burke AP, Virmani R, Goldstein J, and Muller JE, JACC Cardiovasc. Imaging 1, 638 (2008). [PubMed: 19356494]

3. Razansky RN, Rosenthal A, Mallas G, Razansky D, Jaffer FA, and Ntziachristos V, Opt. Express 18, 11372 (2010). [PubMed: 20588998]

4. Bec J, Phipps JE, Gorpas D, Ma D, Fatakdawala H, Margulies KB, Southard JA, and Marcu L, Sci. Rep 7 (2017).

5. Bouma BE, Villiger M, Otsuka K, and Oh W-Y, Biomed. Opt. Express 8, 2660 (2017). [PubMed: 28663897]

6. Tsuboi M, Hayashi A, Ikeda N, Honda H, Kato Y, Ichinose S, and Kato H, Lung Cancer 49, 387 (2005). [PubMed: 15922488]

7. Lee S, Lee MW, Cho HS, Song JW, Nam HS, Oh DJ, Park K, Oh W-Y, Yoo H, and Kim JW, Circ. Cardiovasc. Interv 7, 560 (2014). [PubMed: 25074255]

8. Pahlevaninezhad H, Lee AMD, Ritchie A, Shaipanich T, Zhang W, Ionescu DN, Hohert G, MacAulay C, Lam S, and Lane P, Biomed. Opt. Express 6, 4191 (2015). [PubMed: 26504665]

9. Sherlock BE, Phipps JE, Bec J, and Marcu L, Opt. Lett 42, 3753 (2017). [PubMed: 28957119]

10. Yang VXD, Mao YX, Munce N, Standish B, Kucharczyk W, Marcon NE, Wilson BC, and Vitkin IA, Opt. Lett 30, 1791 (2005). [PubMed: 16092347]

11. Lee MW, Song JW, Kang WJ, Nam HS, Kim TS, Kim S, Oh W-Y, Kim JW, and Yoo H, Sci. Rep 8, 14561 (2018). [PubMed: 30267024]

12. Li J, Ma T, Jing J, Zhang J, Patel PM, Kirk Shung K, Zhou Q, and Chen Z, J. Biomed. Opt 18, 100502 (2013). [PubMed: 24145701]

13. "GRINTECH GmbH gradient index optics," https://www.grintech.de/en/gradient-index-optics/.

14. Xi J, Huo L, Wu Y, Cobb MJ, Hwang JH, and Li X, Opt. Lett 34, 1943 (2009). [PubMed: 19571960]

15. Pahlevaninezhad H, Khorasaninejad M, Huang Y-W, Shi Z, Hariri LP, Adams DC, Ding V, Zhu A, Qiu C-W, Capasso F, and Suter MJ, Nat. Photonics 12, 540 (2018). [PubMed: 30713581]

16. Li J, Fejes P, Lorenser D, Quirk BC, Noble PB, Kirk RW, Orth A, Wood FM, Gibson BC, Sampson DD, and McLaughlin RA, Sci. Rep 8, 14789 (2018). [PubMed: 30287830]

17. Kim G, Domínguez-Caballero JA, and Menon R, Opt. Express 20, 2814 (2012). [PubMed: 22330517]

18. Currie M and McBride R, Proc. SPIE 8970, 89700T (2014).

19. Ma D, Bec J, Yankelevich DR, Gorpas D, Fatakdawala H, and Marcu L, J. Biomed. Opt 19, 066004 (2014). [PubMed: 24898604]

20. "LightForge technical data," http://www.powerphotonic.com/rapid-prototyping/technical-data.

Author Manuscript

Author Manuscript

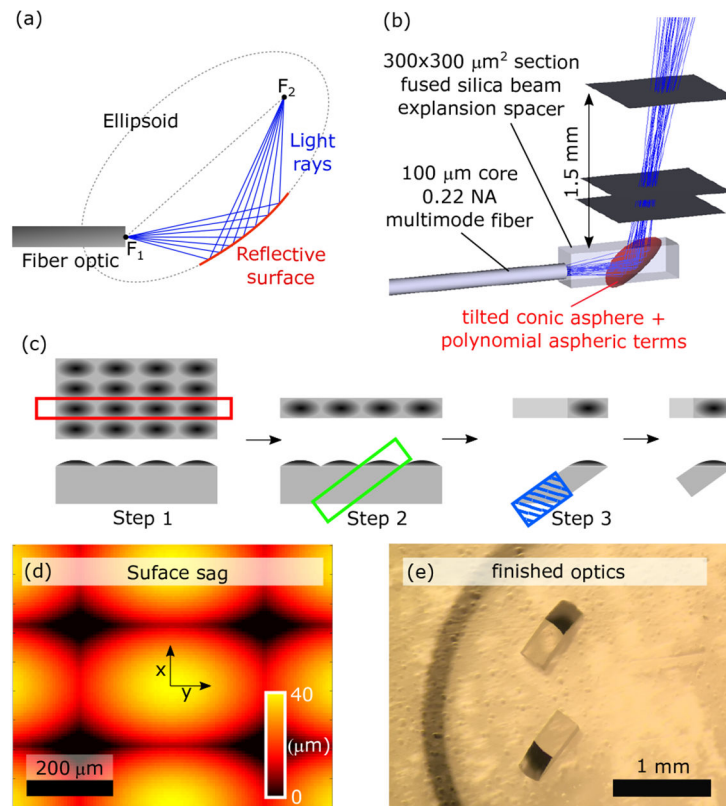Author Manuscript

Author Manuscript

Fig. 1.
Design and manufacturing of freeform optics. (a) Simplified representation: a section of ellipsoid reflects and focuses light rays exiting the fiber core. (b) Zemax simulation model used to perform optimization of the reflective surface. (c) Manufacturing process: the coated array is first cut into individual rows (step 1), then individual elements are cut from each row (step 2) and polished to the designed length (step 3). (d) The surface sag representation of the curved reflective surface highlights that axial and transaxial directions have different curvature radii, thus enabling astigmatism correction. (e) Individual optics after manufacturing completion.
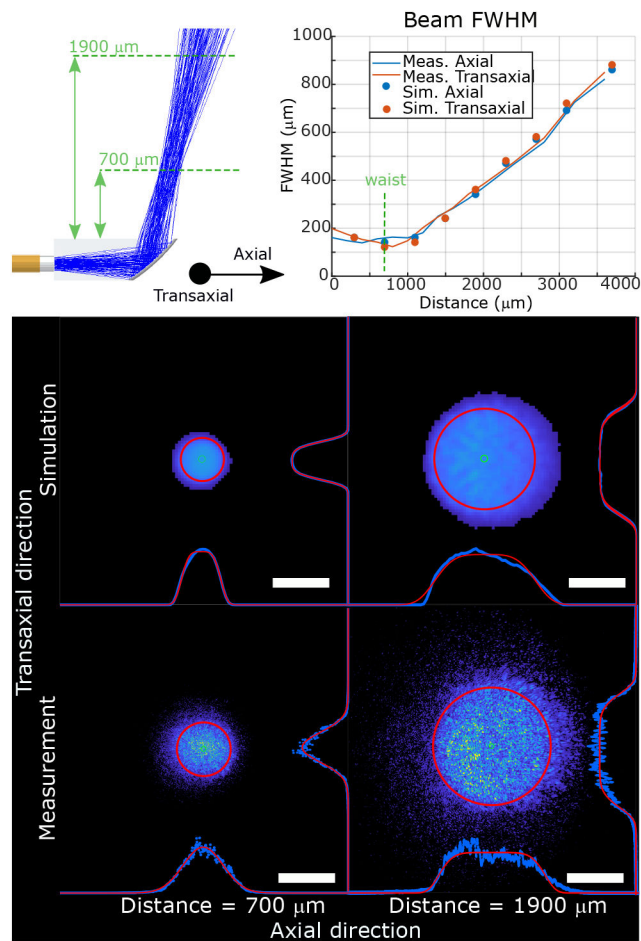
Fig. 2.
Experimentally characterized multimode beam is in good agreement with the beam shape derived from simulations. For each distance, the beam dimensions in the axial and transaxial directions are defined as the full-width half-maximum of the super-Gaussian fit that best approximates the beam profile. For all distances, minimal differences in beam size across the two directions are observed. Red circle: 80% encircled energy. Scale bar: 200 μm.
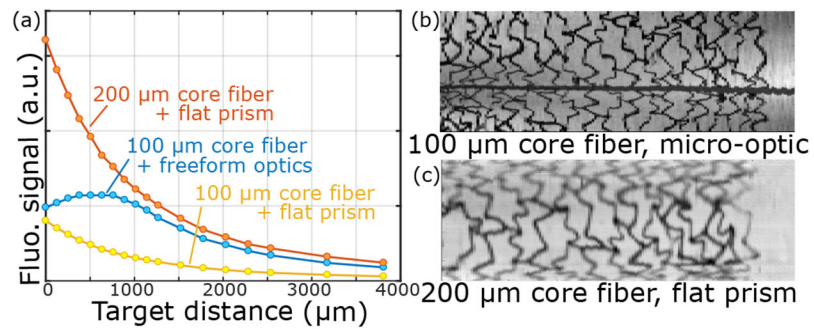
Fig. 3.
Experimental validation of improved collection efficiency and lateral resolution: variation of fluorescence signal in function of distance, for freeform optic and flat prism (a). Fluorescence image of stent illustrating improvements in spatial resolution obtained using the proposed optic (b) with respect to an earlier version of the device (c).
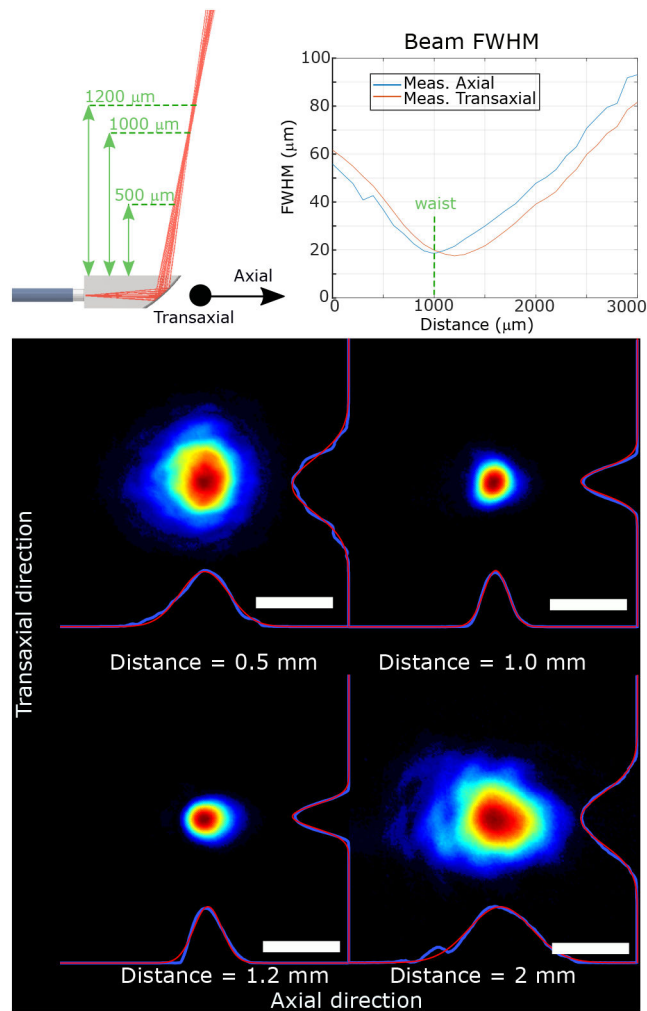
Fig. 4.
Experimental characterization of optical performances for a single-mode beam. The beam profile in the axial and transaxial directions presents low aberrations and a FWHM of less than 20 μm at the waist. For all distances, only minimal differences in beam size across the two directions are observed. Scale bar: 50 μm.
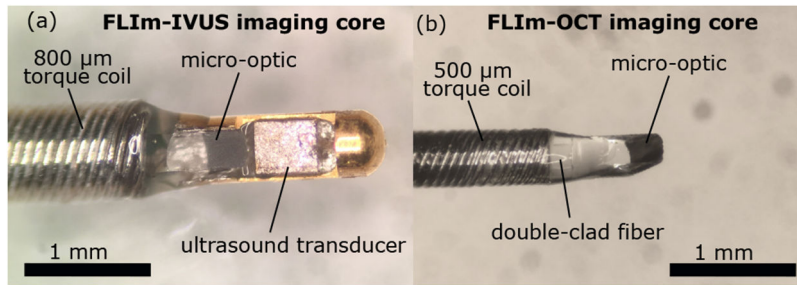
Fig. 5.
Integration of the freeform optics into intravascular imaging devices. FLIm-IVUS intravascular catheter (a). Low-profile FLIm-OCT intravascular catheter core (b).